ACS OMEGA

Open Access

http://pubs.acs.org/journal/acsodf

Article

Adsorption of Cu(II) and Pb(II) in Aqueous Solution by Biochar Composites

Xiaoyan Wang, Xiao Wang, Wanke Chen, Jing Yuan,* and Qianfeng Zhang

Cite This: *ACS Omega* 2025, 10, 13816−13828

Read Online

ACCESS | Metrics & More | Article Recommendations

ABSTRACT: In this study, straw biochar (TB) was prepared by pyrolysis at 500 °C, and biochar composite material (TBS) was prepared by a 1:4 mass ratio with sludge (TS). Scanning electron microscopy and Fourier transform infrared spectroscopy were utilized to characterize the material before and after adsorption. The results demonstrated that TBS possesses significant pore structure characteristics and abundant active functional groups such as hydroxyl, carboxyl, and carbonyl groups, providing a structural basis for its efficient adsorption of heavy metal ions in aqueous solutions. The adsorption performance of the remediation materials for Cu(II) and Pb(II) in aqueous solution was systematically investigated. Experimental data showed that TBS achieved maximum adsorption capacities of 60.86 and 46.98 mg/g for Cu(II) and Pb(II) at equilibrium, respectively, exhibiting superior adsorption efficiency. Through fitting analysis using adsorption kinetic models and isothermal adsorption models, it was found that the pseudo-second-order kinetic model and Freundlich isothermal model could more accurately describe the adsorption process of the two heavy metal ions, indicating that chemical adsorption was the dominant mechanism and characterized by multilayer adsorption. Thermodynamic parameter calculations revealed negative ΔG values and positive ΔH and ΔS values, suggesting that the adsorption process was a spontaneous, entropy-increasing, and endothermic reaction. These research results fully validate the excellent removal capabilities of TBS for Cu(II) and Pb(II). This study has shown that TBS can be considered a promising and cost-effective adsorbent, demonstrating its potential to adsorb heavy metal ions in water.

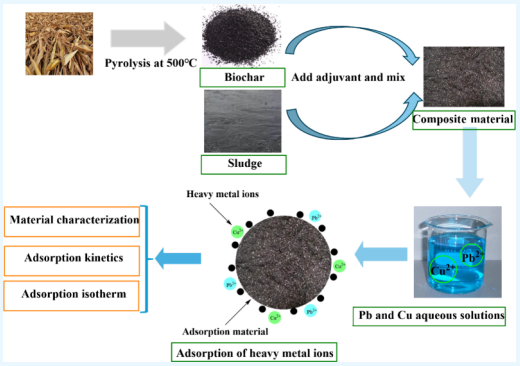

1. INTRODUCTION

As industrialization and urbanization have swiftly emerged, human endeavors such as printing and dyeing, metal mining and smelting, waste treatment, and sewage discharge have intensified, and heavy metal pollution in water bodies has become of increasingly serious concern.[1,2] Heavy metals have the characteristics of high toxicity, nondegradation, long durability, and carcinogenicity. Heavy metal ions such as Pb and Cu in water exhibit significant mobility and easily accumulate in animals and plants through the food chain, thus threatening the lives of humans and other organisms, which has attracted wide attention worldwide.[3−5]

In recent years, various methods have been explored to deal with heavy metal pollution of lead (Pb) and copper (Cu) in water, including chemical precipitation,[6] membrane separation, ion exchange and adsorption, etc.[7−9] Owing to its affordability, adsorption ranks among the most eco-friendly and efficient techniques, is a simple process, and has high efficiency and flexible material design.[10−12] Ganji and Taghavijeloudar used a sand filter to adsorb heavy metals Pb(II) and Cu(II) in water and achieved removal rates of 60% and 55%, respectively.[13] Despite its simplicity of operation, the sand filter requires periodic cleaning and replacement of the filter media, which may cause secondary contamination and increase the complexity of the experiment. Sharma and Devi discovered snail shell powder's capability to efficiently absorb heavy metals Pb(II) and Cu(II) in water, yet its regenerative efficiency was subpar and it was difficult to achieve reuse.[14]

Biochar is a sustainable and renewable green adsorbent that is low cost and widely available and has excellent stability, oxidation resistance, and hydrophobicity. As a multifunctional material with good structural properties containing abundant surface functional groups, pore configurations, extensive specific surface area, and the ability to exchange ions, it exhibits great potential for heavy metal adsorption.[15−17] Solís et al. used coke from pyrolysis of plastics as an adsorbent and discovered its efficacy in absorbing heavy metal Pb in water.[18] The biochars obtained from the pyrolysis of waste marine macroalgae, lobster shell, and waste rapeseed cake have obvious adsorption effects on heavy metal Cu in water.[19−21]

Received: July 25, 2024
Revised: March 6, 2025
Accepted: March 25, 2025
Published: April 2, 2025

https://doi.org/10.1021/acsomega.4c06837
ACS Omega 2025, 10, 13816−13828

Table 1. Physical and Chemical Properties of Straw Biochar and Sludge

sanple	pH	organic matter (g/kg)	cation exchange amount (cmol/kg)	ammonium nitrogen (mg/kg)	available phosphorus (mg/kg)	available potassium (mg/kg)	Pb (mg/kg)	Cu (mg/kg)
straw biochar	8.5	14.35	38.6	12.32	33.85	68.95	0	0
sludge	7.5	19.15	27.5	30.33	45.78	96.33	0	5.23

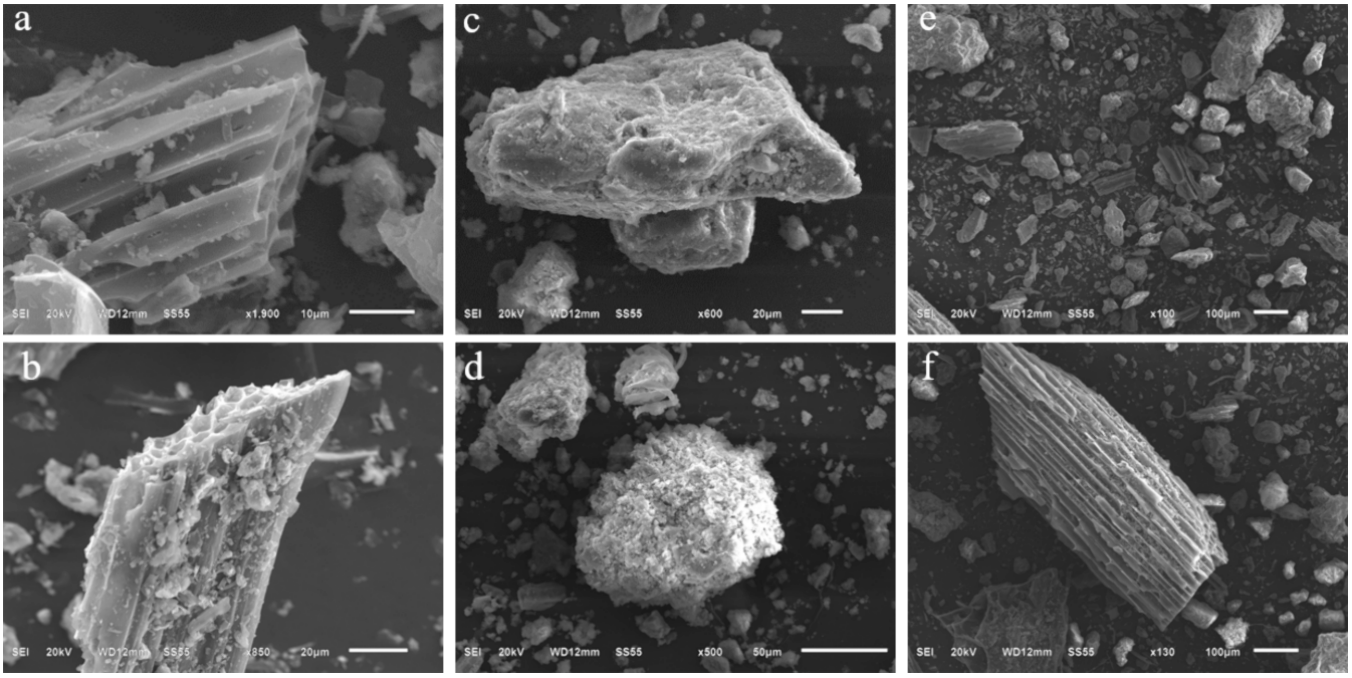

Figure 1. SEM images of (a) TB, (c) TS, and (e) TBS before Cu(II) and Pb(II) adsorption and (b) TB, (d) TS, and (f) TBS after Cu(II) and Pb(II) adsorption.

Research indicates that biochar derived from varied biomass exhibits significant promise and high effectiveness in absorbing heavy metals, such as Pb and Cu. Sludge originating from diverse origins is characterized by its distinctive architecture, extensive specific surface area, and abundant surface functional groups such as hydroxyl, carboxyl, etc.[22] Studies have shown that sludge is a promising adsorbent, which can effectively adsorb heavy metals such as Zn, Cd, and Pb in water.[23−25]

Recent studies mainly focus on the adsorption of lead and copper in water by other biomass materials, and there are few studies on the simultaneous adsorption of lead and copper in water by straw biochar and sludge composite materials. In this study, green straw biochar (TB) and sludge (TS) were chosen as experimental materials for composting and fermentation to obtain biochar composites (TBS). The objective was to investigate the adsorption effects of TB, TS, and TBS on Cu(II) and Pb(II) in contaminated aqueous solutions. Experimental data was analyzed using the adsorption kinetics and isotherm models to investigate how temperature and initial concentration influence the adsorption process and the adsorption characteristics of various repair materials for Cu(II) and Pb(II).

2. MATERIALS AND METHODS

2.1. Experimental Materials. Experimental biochar (TB) is produced through anaerobic pyrolysis at a temperature of 500 °C. The test sludge (TS) was sourced from the Cihu Sewage Treatment Plant located in Anhui Province. Sodium hydroxide (NaOH) and sodium nitrate ($NaNO_3$) were acquired from Shanghai Maclin Biochemical Technology Co., Ltd. Lead chloride ($PbCl_2$) and copper chloride ($CuCl_2$) were acquired from Aladdin Reagent Co., Ltd. EM bacteria and deodorant used in this study were obtained from Zhengzhou Wanwei Biotechnology Co., Ltd. Every reagent employed in the study was of analytically pure (AR) grade. In the experiment, deionized water, processed by a pure water equipment system, served as ultrapure water.

The pH values of straw biochar and sludge were determined by the potentiometric method. The content of organic matter was determined by titration. Determination of cation exchange capacity (CEC) was performed by the spectrophotometric method. The contents of ammonium nitrogen, available phosphorus, and available potassium were determined by a quick nutrient meter. The contents of Cu(II) and Pb(II) were determined by ICP-AES. Table 1 shows the tested physical and chemical characteristics of straw biochar and sludge.

2.2. Experimental Methods. *2.2.1. Sample Preparation.* The proportions of straw biochar (TB) and sludge (TS) were calculated according to a mass ratio of 1:4. Auxiliaries such as quicklime (CaO), bran, deodorants, and EM bacteria were added to improve their physical and chemical properties, reduce odor, and regulate pH. After the mixture was evenly mixed and was subjected to aerobic fermentation for 60 days, the biochar composite repair material was obtained, which is denoted as TBS.

2.2.2. Adsorption Experiment. A 0.5 g sample was weighed into a 100 mL beaker, and an initial concentration of 500 mg/L Pb(II) and 400 mg/L Cu(II) solution (background

https://doi.org/10.1021/acsomega.4c06837
ACS Omega 2025, 10, 13816−13828

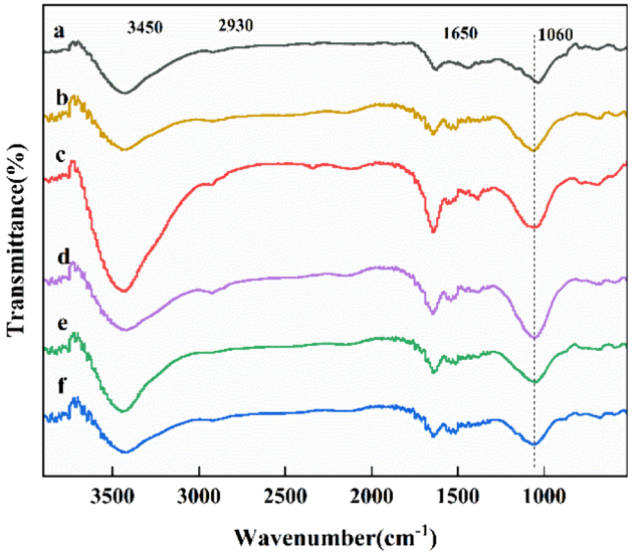

Figure 2. FT-IR images of (a) TB, (c) TS, and (e) TBS prior to Cu(II) and Pb(II) adsorption and (b) TB, (d) TS, and (f) TBS subsequent to Cu(II) and Pb(II) adsorption.

concentration of 0.01 mol/L $NaNO_3$) was added, and the pH was adjusted to 5.5. The samples were spun at 200 rpm for 0, 5, 10, 30, 60, 120, 180, 240, 360, 480, 600, and 720 min at 25 °C. Postcentrifugation, the clear liquid above the sediment was collected, and the levels of Cu(II) and Pb(II) were measured using inductively coupled plasma spectrometry (ICP-AES). The calculation formula of adsorption capacity (q_t, mg/g) at different times is shown in eq 1:

$$q_t = \frac{(C_0 - C_t)}{m} \times \frac{V}{1000} \tag{1}$$

where q_t represents the adsorption capacity at time t (min), mg/g; C_0 denotes the initial concentration of the heavy metal concentration, mg/L; C_t indicates the concentration of the adsorbent at time t (min), mg/L; V is the solution's volume, L; and m is the sample's mass, g.

2.2.3. Adsorption Kinetics. The model of adsorption kinetics is capable of profoundly comprehending how materials absorb heavy metal ions. To thoroughly examine how Cu(II) and Pb(II) adsorb on various adsorbents, three distinct kinetic models were employed, namely, the pseudo-first-order, pseudo-second-order, and Elovich kinetic models, to analyze the adsorption mechanism and adsorption rate during the adsorption process.[26] The formulas are listed in eqs 2–4, respectively.

$$\ln(q_e - q_t) = \ln q_e - K_1 t \tag{2}$$

where K_1 represents the adsorption rate constant in the pseudo-first-order kinetic model, min^{-1}; q_e denotes the adsorption capacity at equilibrium when the concentration is C_e, mg/g; and C_e indicates the adsorbent concentration in the solution at adsorption equilibrium, mg/L.

$$\frac{t}{q_t} = \frac{1}{K_2 q_e^{\,2}} + \frac{1}{q_e} t \tag{3}$$

where K_2 represents the constant rate for the pseudo-second-order kinetic adsorption, g/mg/min.

$$q_t = \frac{1}{\beta}\ln(\alpha\beta) + \frac{1}{\beta}\ln t \tag{4}$$

where α represents the starting rate of adsorption, mg/g·min; and β denotes the constant for desorption, g/mg.

2.2.4. Adsorption Isotherm. A 0.5 g sample was weighed and placed into a 50 mL centrifuge tube, followed by addition of 25 mL of $PbCl_2$ and $CuCl_2$ solutions of different concentrations (with 0.01 mol/L $NaNO_3$ as background). The concentrations were 10, 20, 50, 80, 100, 200, 300, 400, 500, and 600 mg/L, and the pH was adjusted to 5.5. The temperature was oscillated at 15, 25, and 35 °C over a 24 h period. Oscillating at 288, 298 and 308 K for 24 h. Pb and Cu concentrations were determined by centrifuging and collecting the supernatant.

Adsorption isotherms are important methods to elucidate the correlation between the quantity of adsorption and the concentration of the solution at a specific temperature. At temperatures of 288, 298, and 308 K, Langmuir, Freundlich, and Temkin adsorption isothermal models were employed for the purpose of fitting and analyzing the experimental

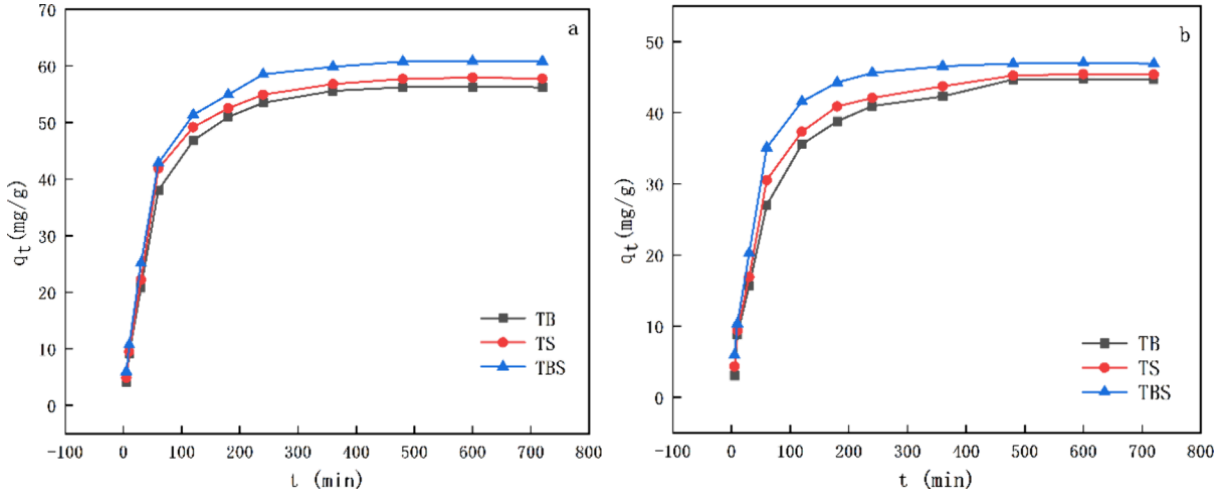

Figure 3. Change curves of the adsorption capacities of TB, TS, and TBS for Cu(II) and Pb(II) with time: (a) the alteration curve for Cu(II) adsorption; (b) the alteration curve for Pb(II) adsorption.

https://doi.org/10.1021/acsomega.4c06837
ACS Omega 2025, 10, 13816−13828

Table 2. Kinetic Parameters of Cu(II) Absorption by TB, TS, and TBS

		pseudo-first-order kinetic model			pseudo-second-order kinetic model			Elovich kinetic model		
sample	$q_{e,exp}$ (mg/g)	$q_{e,cal}$ (mg/g)	$K_1/10^{-1}$ (min^{-1})	R^2	$q_{e,cal}$ (mg/g)	$K_2/10^{-2}$	R^2	α	β	R^2
TB	56.32	51.98	0.13	0.987	64.06	0.028	0.995	3.352	0.084	0.952
TS	57.95	43.59	0.109	0.981	64.68	0.032	0.996	3.723	0.083	0.941
TBS	60.86	51.37	0.126	0.98	67.34	0.033	0.998	4.15	0.08	0.95

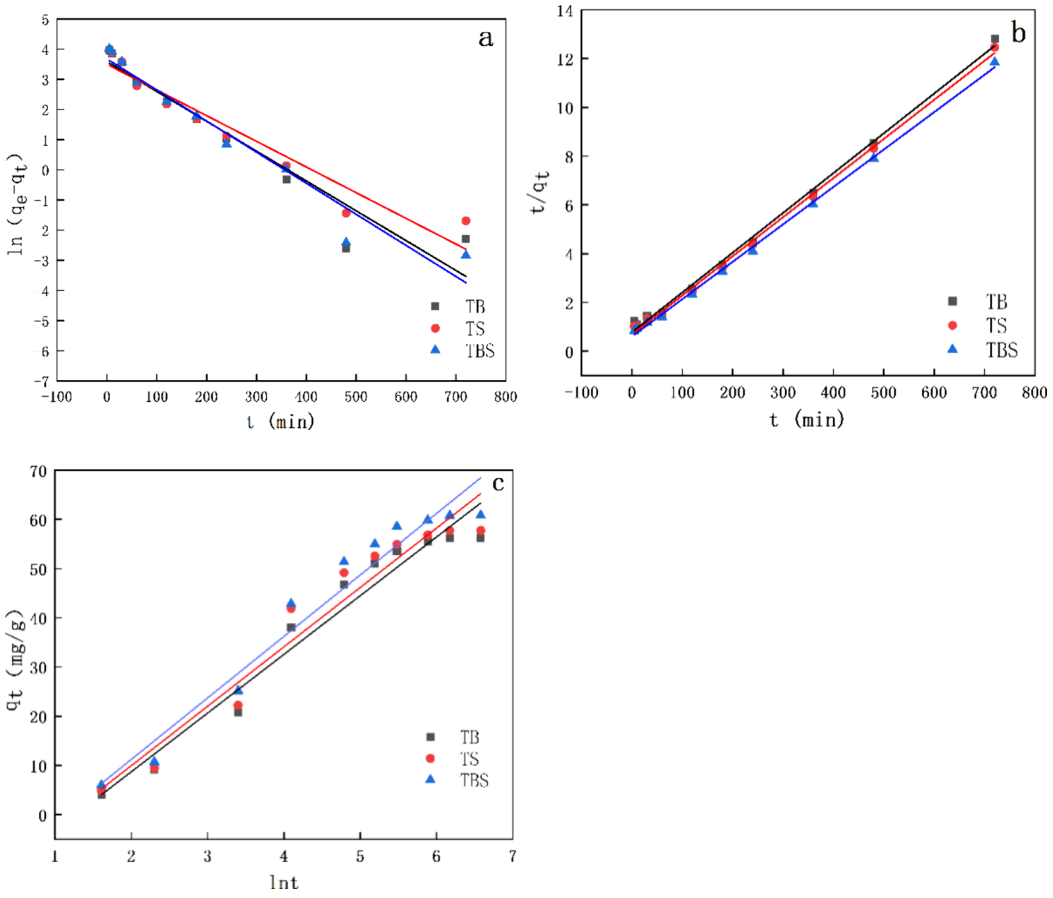

Figure 4. Linear model fitting diagrams of adsorption of Cu(II) by TB, TS, and TBS: (a) pseudo-first-order kinetics; (b) pseudo-second-order dynamics; (c) Elovich dynamics.

data.[27] Equations 5−8 are linearized Langmuir, Freundlich, and Temkin adsorption isotherm models, respectively:

$$\frac{C_e}{q_e} = \frac{C_e}{q_m} + \frac{1}{K_L q_m} \tag{5}$$

where C_e represents the adsorption equilibrium concentration, mg/L; q_e denotes the adsorption amount at adsorption equilibrium, mg/g; q_m is the theoretical maximum adsorption capacity, mg/g; and K_L is the adsorption coefficient, L/mg.

$$\ln q_e = \frac{1}{n}\ln C_e + \ln K_F \tag{6}$$

where K_F is the Freundlich constant, mg/g; and $1/n$ denotes the strength of adsorption.

$$q_e = b\ln C_e + b\ln K_T \tag{7}$$

where b is the Temkin constant, J/mol; and K_T represents the constant of equilibrium adsorption capacity, L/mg.

2.2.5. Adsorption Thermodynamics. Further clarification of how Cu(II) and Pb(II) adsorb on various adsorbents was achieved through the computation of Gibbs free energy (ΔG, kJ/mol), changes in adsorption enthalpy (ΔH, kJ/mol), and entropy (ΔS, J/mol·K).[28−33] The values of ΔH and ΔS can be obtained from the slope and intercept obtained by plotting ln K_d against $1/T$ and performing linear fitting.[34,35] The specific equations are as follows:

$$\Delta G = -RT \ln K_d \tag{8}$$

$$K_d = \frac{C_{ae}}{C_e} \tag{9}$$

$$\ln K_d = -\frac{\Delta H}{RT} + \frac{\Delta S}{R} \tag{10}$$

where T represents the absolute temperature, K; R denotes the ideal gas constant, 8.314 J/K/mol; and K_d is the equilibrium constant. C_{ae} represents the concentration of heavy metal ions on the adsorbent at equilibrium, and C_e represents the concentration of the remaining heavy metal ions in the solution at equilibrium.

https://doi.org/10.1021/acsomega.4c06837
ACS Omega 2025, 10, 13816−13828

Table 3. Kinetic Parameters of Pb(II) Absorption by TB, TS, and TBS

		pseudo-first-order kinetic model			pseudo-second-order kinetic model			Elovich kinetic model		
sample	$q_{e,exp}$ (mg/g)	$q_{e,cal}$ (mg/g)	$K_1/10^{-1}$ (min^{-1})	R^2	$q_{e,cal}$ (mg/g)	$K_2/10^{-2}$	R^2	α	β	R^2
TB	44.73	36.88	0.099	0.933	48.69	0.039	0.998	2.55	0.108	0.971
TS	45.42	31.28	0.090	0.97	48.57	0.049	0.999	3.01	0.109	0.958
TBS	46.98	22.25	0.092	0.888	49.55	0.067	0.999	3.91	0.107	0.932

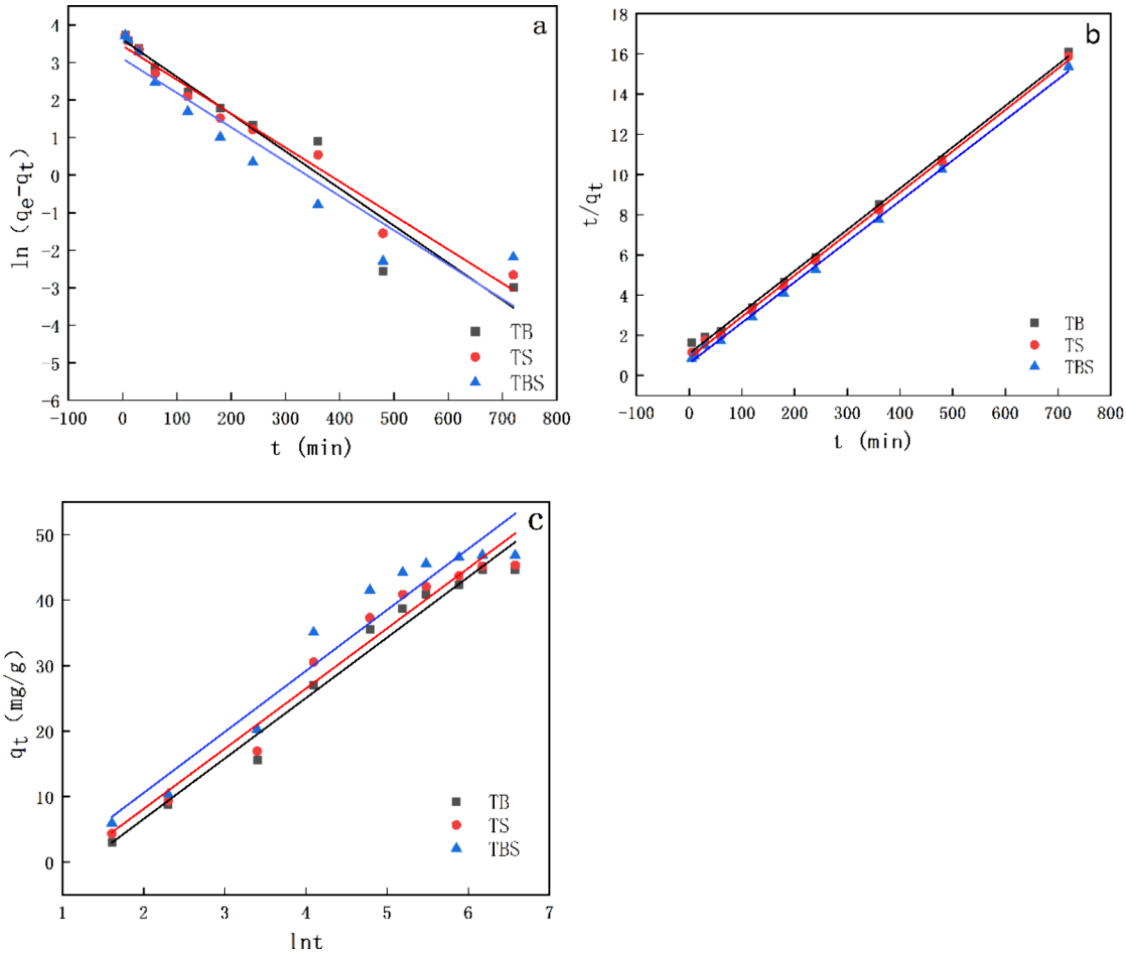

Figure 5. Linear model fitting diagrams of adsorption of Pb(II) by TB, TS, and TBS: (a) pseudo-first-order kinetics; (b) pseudo-second-order dynamics; (c) Elovich dynamics.

2.3. Characterization Techniques. Several experimental instruments were selected to complete the characterization and testing of the materials. The surface functional groups of the material before and after adsorption were detected by an FT-IR spectrometer (Nicolet-6700, USA). The mixing ratio of the sample to KBr was 1:150. Scanning electron microscopy (SEM) (JEM-6480) was employed to examine the adsorbent's surface structure and form.

3. RESULTS AND DISCUSSION

3.1. Material Characterization. *3.1.1. SEM Analysis.* Figure 1a,c,e shows the SEM images of TB, TS, and TBS before adsorption. It can be observed that the TB sample exhibits a high density of pore structures, a smooth and regular surface, and obvious pore structure. TS is irregular and coarse granular, and the particles are packed tightly together with many stacking pores. Figure 1c clearly illustrates that TBS possesses a distinct composition of biochar and sludge. The uneven distribution of biochar and sludge promoted the growth of microorganisms, making TBS have greater porosity, which is conducive to the absorption of the heavy metals Cu(II) and Pb(II). Figure 1b,d,f shows the SEM images of TB, TS, and TBS after adsorption. Post the adsorption of Cu(II) and Pb(II), the material's surface becomes coarse, with numerous particles visibly present in the pores and on its surface. This suggests that the adsorption of Cu(II) and Pb(II) by the adsorbent is effective.

3.1.2. FT-IR Analysis. Materials pre- and post adsorption were analyzed using FT-IR, with the findings presented in Figure 2. The FT-IR spectral analysis of TB, TS, and TBS are similar, indicating that the surface of the adsorbent contains similar functional groups. The wide peak at (3400−3600) cm^{-1} results from a hydroxyl (−OH) stretching vibration peak caused by the carboxyl and hydroxyl functional groups, while the peak at (2800−3000) cm^{-1} arises from the stretching vibration of the sp^3 hybridized −CH, $-CH_2$, and $-CH_3$ bonds on −OH. The peak at (1600−1700) cm^{-1} is caused by compounds containing C=O groups, and the peak at (1020−

https://doi.org/10.1021/acsomega.4c06837
ACS Omega 2025, 10, 13816−13828

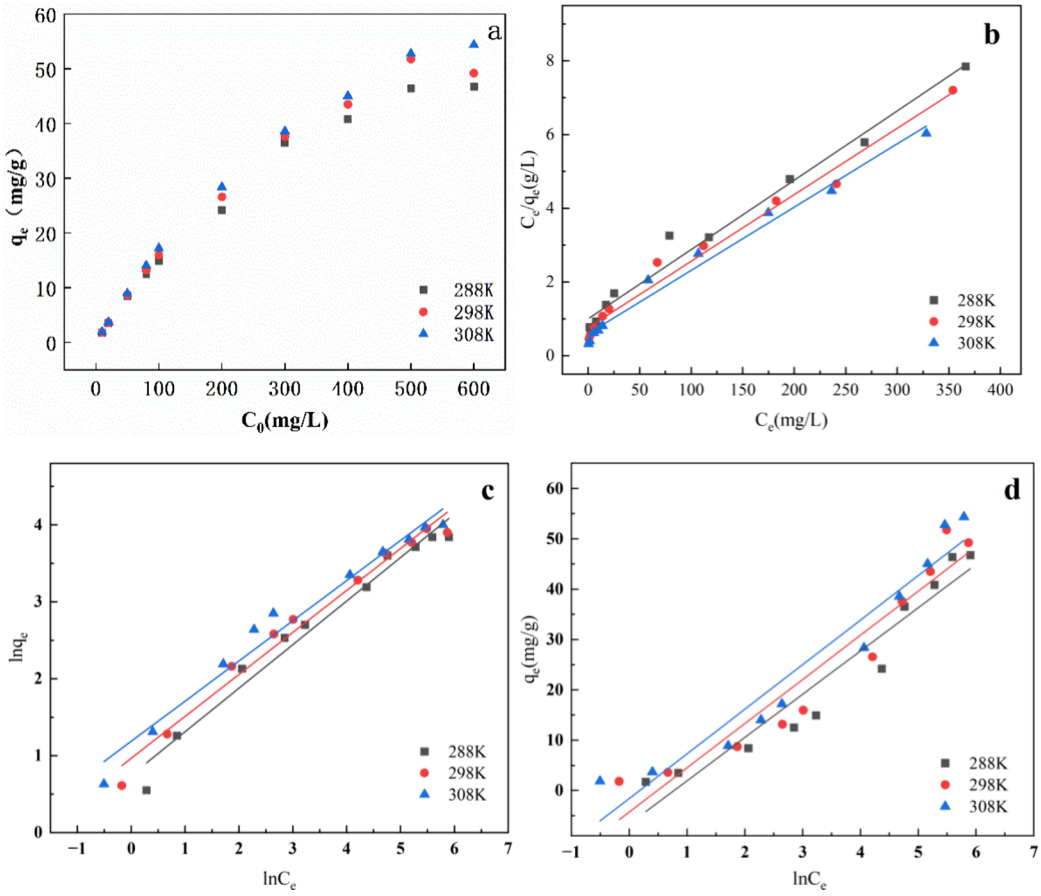

Figure 6. Fitting curves of adsorption of Cu(II) by TB: (a) equilibrium adsorption capacity and initial concentration; (b) Langmuir, (c) Freundlich, and (d) Temkin.

1300) cm^{-1} is caused by compounds containing −C−O groups. The materials after adsorption were characterized. It can be seen that they are slightly shifted from the −OH and −COOH peaks before adsorption, indicating that the oxygen-rich groups such as −OH and −COOH in TB, TS, and TBS are capable of reacting with Cu(II) and Pb(II) in water-based solutions. In the adsorption substance, C, H, and O play roles in the absorption of heavy metal ions.

3.2. Analysis of Adsorption Experimental Data. Figure 3 illustrates the variation in the adsorption abilities of TB, TS, and TBS for Cu(II) and Pb(II) over time. It was observed that their adsorption trends were roughly the same. In the first 60 min, the adsorption capacity increased rapidly and then increased slowly. TBS exhibited a higher capacity for adsorption compared with TB and TS. TB, TS, and TBS demonstrated a gradual increase in their adsorption ability on Cu(II), stabilizing after 180 min, with their maximum equilibrium adsorption capacity hitting 60.86 mg/g (Figure 3a). Regarding the absorption ability of Pb(II) (Figure 3b), it slowly stabilized after a gradual increase over 120−360 min, peaking at an adsorption capacity of 46.98 mg/g, primarily due to the abundance of adsorption sites on TB, TS, and TBS surfaces during the initial adsorption phase. Moreover, there is a concentration difference in the solution, and Cu(II) and Pb(II) ions persist in infiltrating the adsorption site within the material, so the adsorption amount continues to increase. As time progresses, the adsorption site of the material diminishes, thereby achieving a state of equilibrium.[36,37]

3.3. Adsorption Kinetic Analysis. As shown in Table 2 and Figure 4, experimentally measured adsorption capacities $q_{e(exp)}$ for Cu(II) by TB, TS, and TBS were 56.32 57.95, and 60.86 mg/g, respectively. The pseudo-first-order kinetic model determined the equilibrium adsorption quantities $q_{e(cal)}$ to be 51.98 43.59, and 51.37 mg/g, which were significantly different from the actual experimental values. The pseudo-first-order kinetic model falls short in elucidating the adsorption mechanism of Cu(II) by TB, TS, and TBS. The pseudo-second-order kinetic model demonstrated superior performance in fitting the experimental data obtained from the adsorption process, as evidenced by a higher linear determination coefficient (R^2 > 0.99).[38] This model determined that the equilibrium adsorption rates $q_{e(cal)}$ were 56.32, 57.95, and 60.86 mg/g, respectively, aligning more closely with the real experimental figures. Accordingly, the pseudo-second-order kinetic model aptly characterizes the entire adsorption mechanism, and the adsorption process of Cu(II) is predominantly chemisorption. In the Elovich kinetic model, the magnitude of the β value can indicate the degree of adsorbent surface covering the adsorbent and the magnitude of the activation energy of the chemisorption reaction. The smaller the β value is, the higher the activation energy is.[39] The β value of TBS is smaller than those of TB and TS, indicating that TBS has more active adsorption sites and stronger electron donor capacity, and the binding rate of Cu(II) is faster.

Table 3 and Figure 5 display the kinetic parameters of adsorption and the linear model for Pb(II) adsorption by TB,

https://doi.org/10.1021/acsomega.4c06837
ACS Omega 2025, 10, 13816−13828

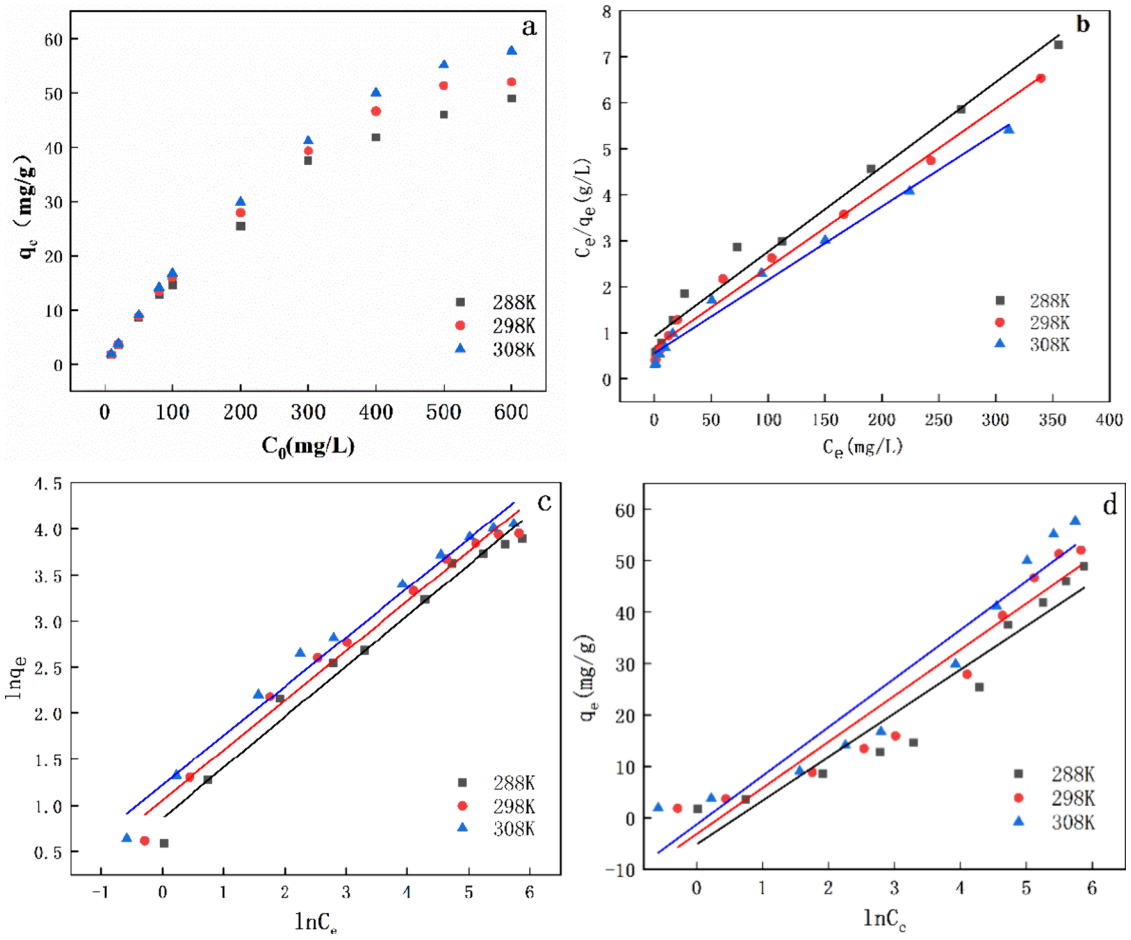

Figure 7. Fitting curves of adsorption of Cu(II) by TS: (a) equilibrium adsorption capacity and initial concentration; (b) Langmuir, (c) Freundlich, and (d) Temkin.

TS, and TBS. The adsorption rates $q_{e(exp)}$ for Pb(II) adsorbed by TB, TS, and TBS were measured to be 44.73, 45.42, and 46.98 mg/g, respectively, aligning closely with the equilibrium absorption rates $q_{e(cal)}$ derived from the pseudo-second-order kinetic model (48.69, 48.57, and 49.55 mg/g), with the linearity determined coefficient $R^2 > 0.99$.[40] Consequently, the adsorption process of Pb(II) by TB, TS, and TBS aligns more closely with the pseudo-second-order kinetic model, involving the movement, swapping, or simultaneous presence of electrons between molecules adsorbed and atoms on the solid surface (or molecules), leading to the creation of adsorption chemical bonds. This adsorption process is usually slow, but the adsorption force is strong and has a certain selectivity. The functional groups, i.e., hydroxyl and carboxyl groups, in TB, TS, and TBS adsorbed materials have ion-exchanged with Cu(II) and Pb(II) ions, so chemisorption plays a predominant role in the adsorption mechanism of Pb(II).[41] The Elovich model is equally apt for characterizing the adsorption dynamics of Pb(II) through TB, TS, and TBS ($R^2 > 0.93$), which further confirms that the adsorption process of TB, TS, and TBS on Pb(II) is mainly affected by chemisorption of the surface-active sites of materials. The β value of TBS is smaller than those of TB and TS, indicating that the binding reaction rate of TBS and Pb(II) is faster.

3.4. Adsorption Isotherm Analysis. To delve into the nature of the adsorption process, including the interaction mechanism between adsorbent and adsorbate, three adsorption isothermal models were chosen to be fitted.[42] Figures 6−8 (panel a) illustrates the variation in the adsorption ability of TB, TS, and TBS to Cu(II) as the initial concentration of Cu(II) alters. As the initial concentration of Cu(II) rose, the adsorption capacities of TB, TS, and TBS for Cu(II) increased gradually. Research revealed an enhancement in the absorption ability of TB, TS, and TBS on Cu(II) correlated with rising temperatures. At temperatures of 288, 298, and 308 K, the adsorption capacity of TB for Cu(II) ranges from 53.19 to 58.24 mg/g, that of TS for Cu(II) ranges from 54.26 to 62.7 mg/g, and that of TBS for Cu(II) ranges from 55.19 to 65.27 mg/g.

Figures 6−8 (panels b−d) and Table 4 display the linear fitting chart and the isotherm model parameters for the adsorption of Cu(II) by TB, TS, and TBS, respectively. In the Langmuir adsorption isotherm, K_L is linked to adsorption capacity: a higher K_L value indicates a more robust adsorption capacity. At different temperatures, the K_L values of TBS were greater than those of TB and TS, indicating that TBS has a stronger adsorption capacity for Cu(II). In the Freundlich adsorption isotherm model, the parameter $1/n$ is of particular significance in characterizing the nature of the adsorption process.[43,44] When $1/n > 1$, it usually indicates that the adsorption process is favorable; when $1/n < 1$, it is unfavorable; and when $1/n = 1$, the adsorption process is irreversible. The $1/n$ values of TB, TS, and TBS in the adsorption process of Cu(II) are all less than 1, indicating that

https://doi.org/10.1021/acsomega.4c06837
ACS Omega 2025, 10, 13816−13828

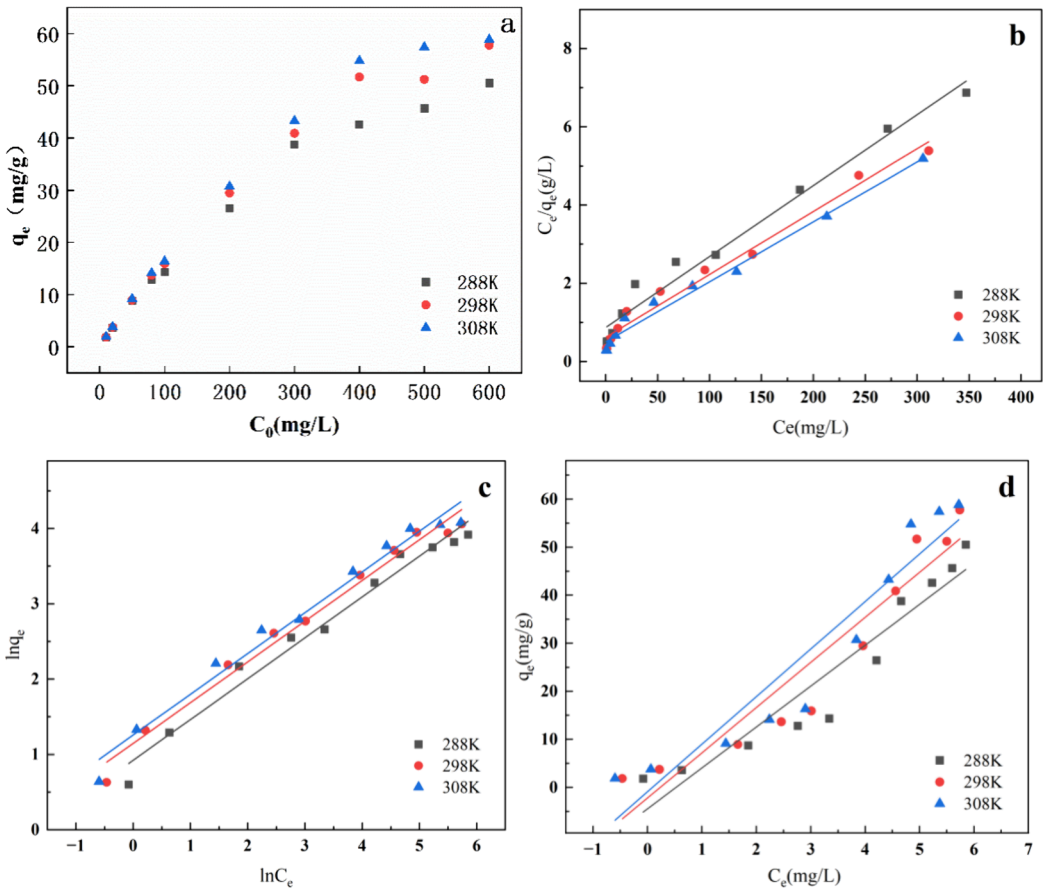

Figure 8. Fitting curves of adsorption of Cu(II) by TBS: (a) equilibrium adsorption capacity and initial concentration; (b) Langmuir, (c) Freundlich, and (d) Temkin.

Table 4. Isotherm Fitting Parameters of Cu(II) Adsorption by TB, TS, and TBS

		Langmuir			Freundlich			Temkin		
sample	T (K)	$q_{m,cal}$ (mg/g)	K_L (L/mg)	R^2	$1/n$	K_F	R^2	b (J/mol)	K_T (J/mg)	R^2
TB	288	53.19	0.019	0.979	0.566	2.105	0.99	8.59	0.462	0.919
	298	55.46	0.024	0.98	0.545	2.624	0.987	8.77	0.618	0.913
	308	58.24	0.029	0.971	0.522	3.277	0.981	8.86	0.84	0.930
TS	288	54.26	0.02	0.979	0.549	2.368	0.986	8.49	0.545	0.911
	298	57.8	0.025	0.986	0.54	2.88	0.988	8.97	0.702	0.916
	308	62.7	0.029	0.986	0.533	3.398	0.989	9.46	0.871	0.918
TBS	288	55.19	0.021	0.974	0.543	2.513	0.975	8.52	0.593	0.902
	298	62.23	0.026	0.978	0.541	3.149	0.981	9.4	0.793	0.895
	308	65.27	0.03	0.983	0.541	3.518	0.976	9.9	0.914	0.897

Table 5. Isotherm Fitting Parameters for Pb(II) Adsorption by TB, TS, and TBS

		Langmuir			Freundlich			Temkin		
sample	T (K)	$q_{m,cal}$ (mg/g)	K_L (L/mg)	R^2	$1/n$	K_F	R^2	b (J/mol)	K_T (J/mg)	R^2
TB	288	38.48	0.016	0.937	0.469	2.154	0.97	5.46	0.598	0.854
	298	43.46	0.018	0.939	0.468	2.567	0.981	6.06	0.735	0.857
	308	47.96	0.021	0.949	0.459	3.121	0.987	6.45	1.001	0.852
TS	288	41.49	0.016	0.96	0.511	1.963	0.979	6.35	0.478	0.895
	298	45.29	0.019	0.96	0.489	2.488	0.99	6.58	0.666	0.886
	308	48.52	0.025	0.97	0.478	3.069	0.985	6.95	0.906	0.9
TBS	288	42.97	0.017	0.967	0.581	2.353	0.992	6.98	0.348	0.856
	298	46.71	0.020	0.973	0.506	2.834	0.988	7.02	0.624	0.907
	308	48.38	0.031	0.979	0.478	3.28	0.974	7.18	0.984	0.928

https://doi.org/10.1021/acsomega.4c06837
ACS Omega 2025, 10, 13816−13828

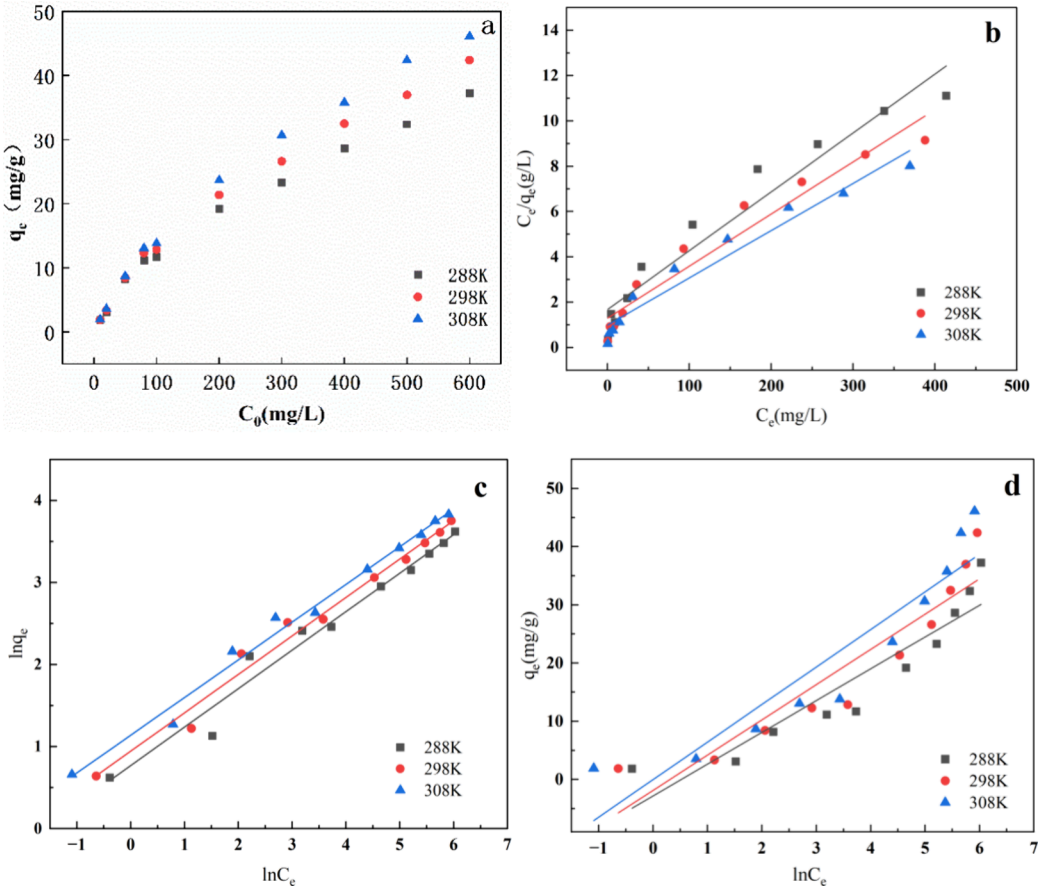

Figure 9. Fitting curves of adsorption of Pb(II) by TB: (a) equilibrium adsorption capacity and initial concentration; (b) Langmuir, (c) Freundlich, and (d) Temkin.

the adsorption is favorable and easy to carry out. The results obtained from the Freundlich isotherm model are more closely aligned with the observed adsorption behavior, indicating that this model is more suitable for describing the adsorption process, which is likely to be multilayer adsorption.[45]

Figures 9−11 (panel a) illustrate that as the initial concentration of Pb(II) rises, the adsorption efficiencies of TB, TS, and TBS on Pb(II) escalate, with the adsorption impact intensifying as the temperature rises. The findings indicated that temperature increase was beneficial to the adsorption of Pb(II) by TB, TS, and TBS, and the adsorption of Pb(II) by TBS was the most obvious. As illustrated in Figures 9−11 (panels b−d) and Table 5, at temperatures of 288, 298, and 308 K, the adsorption capacity of TB for Pb(II) ranges from 38.48 to 47.96 mg/g, while that of TS for Pb(II) ranges from 41.49 to 48.52 mg/g. The adsorption capacity of TBS for Pb(II) ranges from 42.97 to 48.38 mg/g, with the adsorption capacity of TBS for Pb(II) being notably stronger. The Freundlich model has the best fitting effect, and the adsorption of lead by TB, TS, and TBS is mainly multilayer adsorption. All $1/n$ values fall below 1, signifying the simplicity of the Pb(II) adsorption procedure. The K_F values of TBS were all greater than those of TB and TS, indicating that TBS has a greater capacity to adsorb Pb(II) and Cu(II).

3.5. Adsorption Thermodynamic Analysis. The parameters of the adsorption thermodynamic functions of TB, TS, and TBS for Cu(II) and Pb(II) are shown in Tables 6 and 7, and their linear fits are shown in Figure 12. The Gibbs free energy (ΔG) is negative at temperatures of 288, 298, and 308 K, indicating that the uptake of Cu(II) and Pb(II) by TB, TS, and TBS occurs naturally. As the temperature increases, the ΔG value decreases, indicating that a more spontaneous adsorption process occurs at high temperatures, mainly because chemical adsorption is more dominant than physical adsorption.[46] The adsorption enthalpies (ΔH) for TB, TS, and TBS are all positive, indicating that this adsorption process is heat-absorbing.[47,48] With the increase in temperature, the thermal movement of Cu(II) and Pb(II) intensifies, thus contributing to the adsorption process. The enthalpy change ΔH values of the three repair materials in the tables are all more than 20 kJ/mol, which further proves that the adsorption process is mainly chemical adsorption.[49] The adsorption entropies (ΔS) of TB, TS, and TBS are all positive, indicating that the disorder of the system increases during the adsorption of Cu(II) and Pb(II) by TB, TS, and TBS. This increase in the degree of disorder indicates that the adsorption process causes a change of state at the molecular level and also reflects that they have a strong adsorption affinity for Cu(II) and Pb(II).[50,51]

4. CONCLUSIONS

This study prepared the composite remediation material TBS through composting fermentation of biochar and sludge and systematically investigated its adsorption characteristics and mechanisms for Cu(II) and Pb(II) in water. By examining the materials pre- and post adsorption, one reveals clear pore configurations and abundant functional groups such as hydroxyl, carboxyl, and carbonyl, capable of efficiently

https://doi.org/10.1021/acsomega.4c06837
ACS Omega 2025, 10, 13816−13828

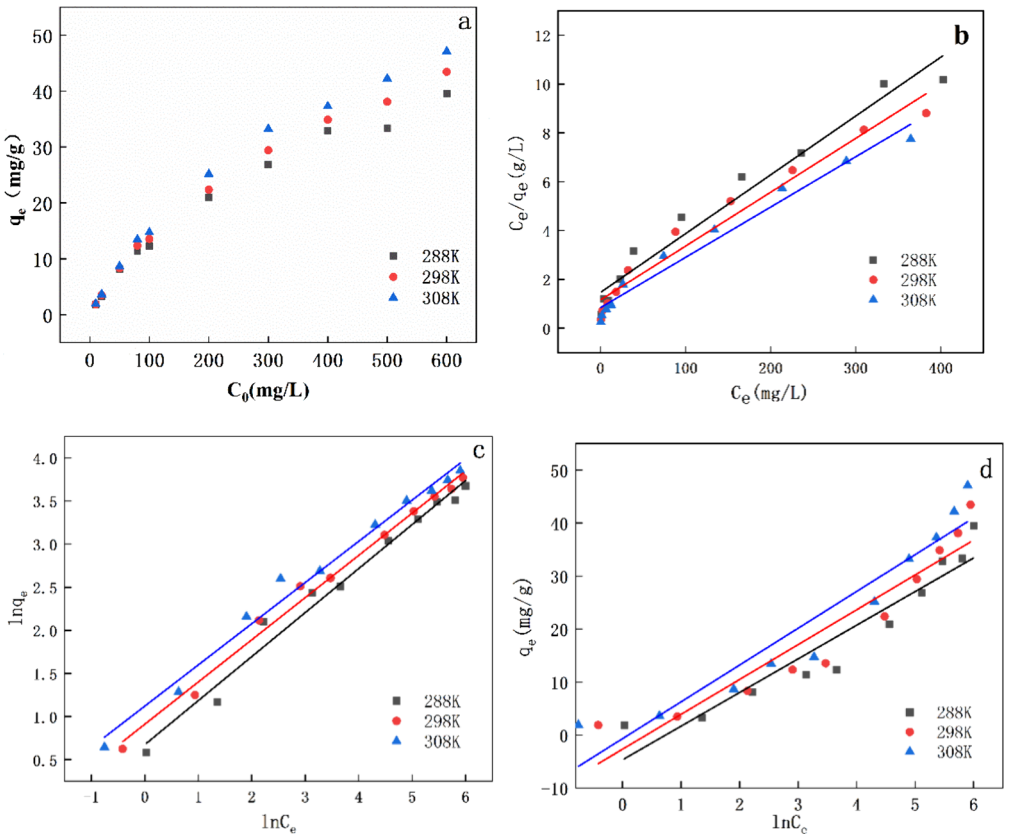

Figure 10. Fitting curves of adsorption of Pb(II) by TS: (a) equilibrium adsorption capacity and initial concentration; (b) Langmuir, (c) Freundlich, and (d) Temkin.

Table 6. Thermodynamic Parameters of Cu(II) Adsorption by TB, TS, and TBS

			ΔG (kJ/mol)			
sample	ΔH (kJ/mol)	ΔS (J/mol/K)	288 K	298 K	308 K	R^2
TB	32.5	128.58	−4.49	−5.92	−7.05	0.986
TS	23.6	100.06	−5.21	−6.22	−7.23	0.999
TBS	20.38	90.16	−5.48	−6.69	−7.28	0.871

Table 7. Thermodynamic Parameters of Pb(II) Adsorption by TB, TS, and TBS

			ΔG (kJ/mol)			
sample	ΔH (kJ/mol)	ΔS (J/mol/K)	288 K	298 K	308 K	R^2
TB	33.27	131.69	−4.57	−6.15	−7.19	0.965
TS	31.38	127.07	−5.18	−6.57	−7.71	0.991
TBS	26.82	114.6	−6.27	−7.14	−8.57	0.933

absorbing heavy metal ions, thus diminishing the contents of Cu(II) and Pb(II) in water. The adsorption kinetics study showed that the adsorption process of Cu(II) and Pb(II) could be divided into two stages: rapid adsorption (0−60 min) and equilibrium adsorption, and the adsorption effect of TBS on Cu(II) and Pb(II) was better. The adsorption capacities at equilibrium were 60.86 and 46.98 mg/g, respectively. By changing the initial concentration and temperature of the solution, it was found that the increase of temperature had a positive effect on the absorption of Cu(II) and Pb(II), and the maximum absorption capacities were 65.27 and 48.38 mg/g, respectively. The experimental data were fitted by an adsorption kinetic model and adsorption isotherm model. Adsorption kinetics studies show that the fitting degree of the pseudo-second-order kinetic model ($R^2 > 0.99$) is significantly superior to that of the pseudo-first-order model, indicating that the adsorption process is predominantly governed by chemical adsorption. The isothermal adsorption experiments showed that the Freundlich model ($1/n < 1$) provides a better description of the adsorption process, suggesting the presence of heterogeneous adsorption sites on the surface of TBS and that multilayer adsorption is the main characteristic. The calculation of thermodynamic parameters shows that ΔG is negative and ΔH and ΔS are positive, which confirms that the adsorption process is a spontaneous and endothermic entropy-driven process, and the disorder degree of the solid−liquid interface increases. Compared with TB and TS, TBS has a better adsorption effect on Cu(II) and Pb(II), and the adsorption efficiency is higher. In summary, TBS shows significant promise for future applications in the removal of

https://doi.org/10.1021/acsomega.4c06837
ACS Omega 2025, 10, 13816−13828

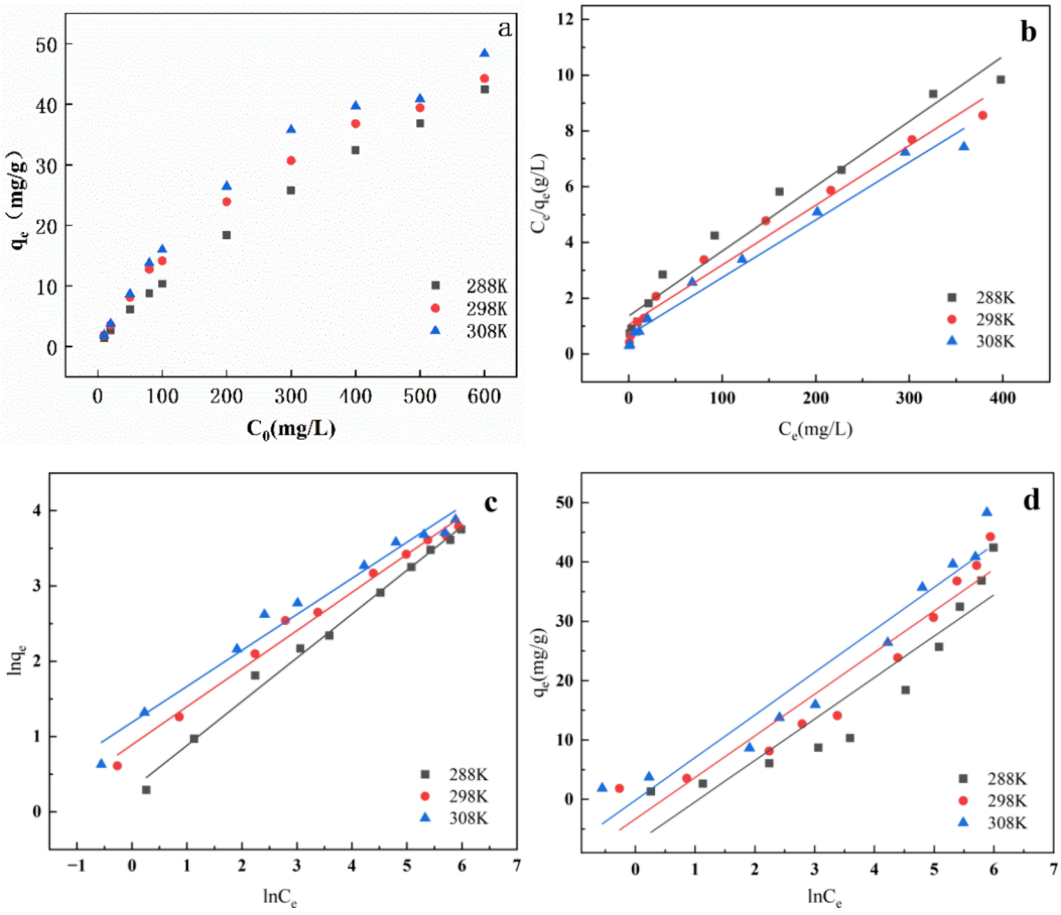

Figure 11. Fitting curves of adsorption of Pb(II) by TBS: (a) equilibrium adsorption capacity and initial concentration; (b) Langmuir, (c) Freundlich, and (d) Temkin.

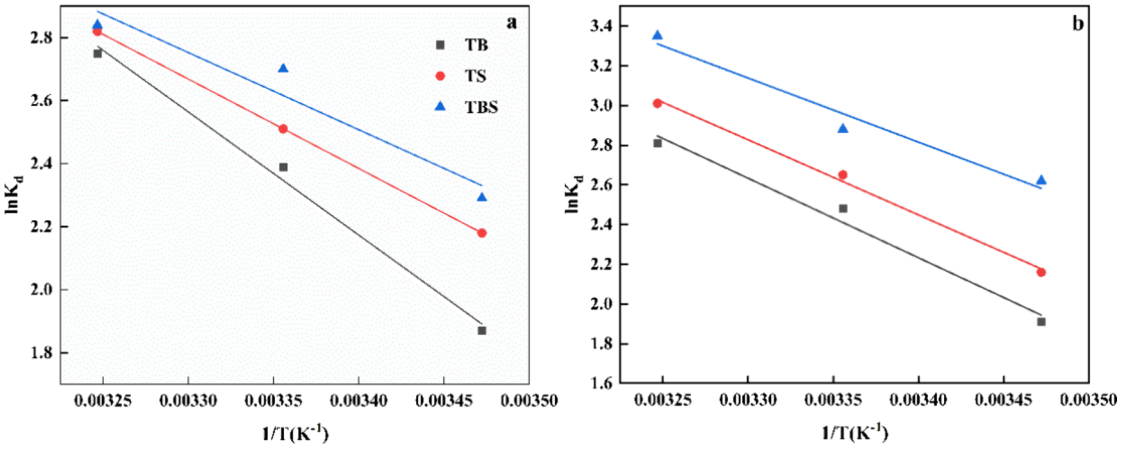

Figure 12. Thermodynamic parameter fitting diagrams for adsorption of Cu(II) and Pb(II) by TB, TS, and TBS: (a) Cu(II); (b) Pb(II).

heavy metal ions, and when paired with other technologies under optimal conditions, it can effectively eliminate heavy metal ions from water.

AUTHOR INFORMATION

Corresponding Author

Jing Yuan − *Department of Civil Engineering, Tongling University, Tongling 244000, China; Department of Civil Engineering, Manitoba University, Winnipeg, MB R3T2N2, Canada;* orcid.org/0000-0002-8839-925X; Email: 154427@tlu.edu.cn

Authors

Xiaoyan Wang − *Institute of Molecular Engineering and Applied Chemistry, Anhui University of Technology, Ma'anshan 243002, China*

Xiao Wang − *Institute of Molecular Engineering and Applied Chemistry, Anhui University of Technology, Ma'anshan 243002, China*

https://doi.org/10.1021/acsomega.4c06837
ACS Omega 2025, 10, 13816−13828

Wanke Chen − *Institute of Molecular Engineering and Applied Chemistry, Anhui University of Technology, Ma'anshan 243002, China*

Qianfeng Zhang − *Institute of Molecular Engineering and Applied Chemistry, Anhui University of Technology, Ma'anshan 243002, China;* orcid.org/0000-0003-0512-8532

Complete contact information is available at: https://pubs.acs.org/10.1021/acsomega.4c06837

Notes

The authors declare no competing financial interest.

■ ACKNOWLEDGMENTS

This research project was partially supported by the National Natural Science Foundation of China (42271301), the Anhui University Excellent Research and Innovation Project (No. 2022AH010094), and Spatial Information Acquisition and Application Joint Laboratory of Anhui Province (No. 2024tlxykjxx04). The authors appreciate the reviewers for their invaluable comments that have led to significant improvements in the paper.

■ REFERENCES

(1) Zhang, L.; Zeng, Y.; Cheng, Z. Removal of Heavy Metal Ions Using Chitosan and Modified Chitosan: A Review. *J. Mol. Liq.* **2016**, *214*, 175−191.

(2) Wanjiya, M.; Zhang, J. C.; Wu, B.; Yin, M. J.; An, Q. F. Nanofiltration Membranes for Sustainable Removal of Heavy Metal Ions from Polluted Water: A Review and Future Perspective. *Desalination* **2024**, *578*, No. 117441.

(3) Feng, X.; Long, R.; Wang, L.; Liu, C.; Bai, Z.; Liu, X. A Review on Heavy Metal Ions Adsorption from Water by Layered Double Hydroxide and Its Composites. *Sep. Purif. Technol.* **2022**, *284*, No. 120099.

(4) Jiang, C.; Wang, X.; Wang, G.; Hao, C.; Li, X.; Li, T. Adsorption Performance of a Polysaccharide Composite Hydrogel Based on Crosslinked Glucan/Chitosan for Heavy Metal Ions. *Compos. Part B Eng.* **2019**, *169* (March), 45−54.

(5) Ahmadijokani, F.; Molavi, H.; Peyghambari, A.; Shojaei, A.; Rezakazemi, M.; Aminabhavi, T. M.; Arjmand, M. Efficient Removal of Heavy Metal Ions from Aqueous Media by Unmodified and Modified Nanodiamonds. *J. Environ. Manage.* **2022**, *316*, No. 115214.

(6) Benalia, M. C.; Youcef, L.; Bouaziz, M. G.; Achour, S.; Menasra, H. Removal of Heavy Metals from Industrial Wastewater by Chemical Precipitation: Mechanisms and Sludge Characterization. *Arab. J. Sci. Eng.* **2022**, *47* (5), 5587−5599.

(7) Nemati, M.; Hosseini, S. M.; Shabanian, M. Novel Electrodialysis Cation Exchange Membrane Prepared by 2-Acrylamido-2-Methylpropane Sulfonic Acid; Heavy Metal Ions Removal. *J. Hazard. Mater.* **2017**, *337*, 90−104.

(8) Xiang, H.; Min, X.; Tang, C. J.; Sillanpää, M.; Zhao, F. Recent Advances in Membrane Filtration for Heavy Metal Removal from Wastewater: A Mini Review. *J. Water Process Eng.* **2022**, *49*, No. 103023.

(9) Basem, A.; Jasim, D. J.; Majdi, H. S.; Mohammed, R. M.; Ahmed, M.; Al-Rubaye, A. H.; Kianfar, E. Adsorption of Heavy Metals from Wastewater by Chitosan: A Review. *Results Eng.* **2024**, *23* (April), No. 102404.

(10) Baby, R.; Saifullah, B.; Hussein, M. Z. Carbon Nanomaterials for the Treatment of Heavy Metal-Contaminated Water and Environmental Remediation. *Nanoscale Res. Lett.* **2019**, *14* (1), 341.

(11) Shaikh, R. B.; Saifullah, B.; ur Rehman, F.; Shaikh, R. I. Greener Method for the Removal of Toxic Metal Ions from the Wastewater by Application of Agricultural Waste as an Adsorbent. *Water* **2018**, *10* (10), 1316.

(12) Baby, R.; Saifullah, B.; Hussein, M. Z. Palm Kernel Shell as an Effective Adsorbent for the Treatment of Heavy Metal Contaminated Water. *Sci. Rep.* **2019**, *9* (1), 1−11.

(13) Ganji, H.; Taghavijeloudar, M. Efficient Adsorption of Lead and Copper from Water by Modification of Sand Filter with a Green Plant-Based Adsorbent: Adsorption Kinetics and Regeneration. *Environ. Res.* **2024**, *259* (July), No. 119529.

(14) Sharma, A.; Devi, I. Biosorption of Heavy Metal Ions from Aqueous Effluents Utilising Snail Shell Dust as a Biomaterial. *Environ. Dev. Sustainability* **2024**, *26*, 31879−31896.

(15) Li, H.; Dong, X.; da Silva, E. B.; de Oliveira, L. M.; Chen, Y.; Ma, L. Q. Mechanisms of Metal Sorption by Biochars: Biochar Characteristics and Modifications. *Chemosphere* **2017**, *178*, 466−478.

(16) Wang, H.; Du, Y.; Song, Y.; Zhang, H. Preparation, Characterisation and Adsorption Performance of KOH-Modified Palm Fibre, Platanus Bark and Sesame Stem Biochar. *Int. J. Environ. Sci. Technol.* **2024**, *22*, 2613−2624.

(17) Rassaei, F. Methane Emissions and Rice Yield in a Paddy Soil: The Effect of Biochar and Polystyrene Microplastics Interaction. *Paddy Water Environ.* **2023**, *21* (1), 85−97.

(18) Solís, R. R.; Martín-Lara, M. A.; Ligero, A.; Balbís, J.; Blázquez, G.; Calero, M. Revalorizing a Pyrolytic Char Residue from Post-Consumer Plastics into Activated Carbon for the Adsorption of Lead in Water. *Appl. Sci.* **2022**, *12* (16), 8032.

(19) Poo, K. M.; Son, E. B.; Chang, J. S.; Ren, X.; Choi, Y. J.; Chae, K. J. Biochars Derived from Wasted Marine Macro-Algae (Saccharina Japonica and Sargassum Fusiforme) and Their Potential for Heavy Metal Removal in Aqueous Solution. *J. Environ. Manage.* **2018**, *206*, 364−372.

(20) Ma, J.; Huang, W.; Zhang, X.; Li, Y.; Wang, N. The Utilization of Lobster Shell to Prepare Low-Cost Biochar for High-Efficient Removal of Copper and Cadmium from Aqueous: Sorption Properties and Mechanisms. *J. Environ. Chem. Eng.* **2021**, *9* (1), No. 104703.

(21) Mazurek, K.; Drużyński, S.; Kiełkowska, U.; Wróbel-Kaszanek, A.; Igliński, B.; Cichosz, M. The Application of Pyrolysis Biochar Obtained from Waste Rapeseed Cake to Remove Copper from Industrial Wastewater: An Overview. *Energies* **2024**, *17* (2), 498.

(22) Xu, K.; Li, L.; Huang, Z.; Tian, Z.; Li, H. Efficient Adsorption of Heavy Metals from Wastewater on Nanocomposite Beads Prepared by Chitosan and Paper Sludge. *Sci. Total Environ.* **2022**, *846* (June), No. 157399.

(23) Nguyen, K. M.; Nguyen, B. Q.; Nguyen, H. T.; Nguyen, H. T. H. Adsorption of Arsenic and Heavy Metals from Solutions by Unmodified Iron-Ore Sludge. *Appl. Sci.* **2019**, *9* (4), 619.

(24) Wang, Q.; Li, J. S.; Poon, C. S. Recycling of Incinerated Sewage Sludge Ash as an Adsorbent for Heavy Metals Removal from Aqueous Solutions. *J. Environ. Manage.* **2019**, *247*, 509−517.

(25) Kurniawan, T. A.; Lo, W.; Othman, M. H. D.; Goh, H. H.; Chong, K. K. Biosorption of Heavy Metals from Aqueous Solutions Using Activated Sludge, Aeromasss Hydrophyla, and Branhamella Spp Based on Modeling with GEOCHEM. *Environ. Res.* **2022**, *214* (P4), No. 114070.

(26) Li, R.; Wang, J. J.; Zhang, Z.; Awasthi, M. K.; Du, D.; Dang, P.; Huang, Q.; Zhang, Y.; Wang, L. Recovery of Phosphate and Dissolved Organic Matter from Aqueous Solution Using a Novel CaO-MgO Hybrid Carbon Composite and Its Feasibility in Phosphorus Recycling. *Sci. Total Environ.* **2018**, *642*, 526−536.

(27) Al-Ghouti, M. A.; Da'ana, D. A. Guidelines for the Use and Interpretation of Adsorption Isotherm Models: A Review. *J. Hazard. Mater.* **2020**, *393*, No. 122383.

(28) Tran, H. N. Improper Estimation of Thermodynamic Parameters in Adsorption Studies with Distribution Coefficient KD (qe/Ce) or Freundlich Constant (KF): Considerations from the Derivation of Dimensionless Thermodynamic Equilibrium Constant and Suggestions. *Adsorption Science & Technology.* **2022**, *2022*, 23.

(29) Mudhoo, A.; Pittman, C. U. Adsorption Data Modeling and Analysis Under Scrutiny: A Clarion Call to Redress Recently Found Troubling Flaws. *Chem. Eng. Res. Des.* **2023**, *192*, 371.

(30) Lima, E. C.; Hosseini-Bandegharaei, A.; Moreno-Piraján, J. C.; Anastopoulos, I. A critical review of the estimation of the thermodynamic parameters on adsorption equilibria. Wrong use of equilibrium constant in the Van't Hoof equation for calculation of thermodynamic parameters of adsorption. *J. Mol. Liq.* **2019**, *273*, 425−434.
(31) Ghosal, P. S.; Gupta, A. K. Determination of thermodynamic parameters from Langmuir isotherm constant-revisited. *J. Mol. Liq.* **2016**, 137.
(32) Zhou, X.; Zhou, X. The unit problem in the thermodynamic calculation of adsorption using the langmuir equation. *Chem. Eng. Commun.* **2014**, *201* (11), 1459−1467.
(33) Salvestrini, S.; Ambrosone, L.; Kopinke, F. D. Some mistakes and misinterpretations in the analysis of thermodynamic adsorption data. *J. Mol. Liq.* **2022**, *352*, No. 118762.
(34) Salman, M.; Athar, M.; Farooq, U. Biosorption of heavy metals from aqueous solutions using indigenous and modified lignocellulosic materials. *Rev. Environ. Sci. Biotechnol.* **2015**, *14* (2), 211−228.
(35) Sahmoune, M. N. Evaluation of thermodynamic parameters for adsorption of heavy metals by green adsorbents. *Environmental Chemistry Letters.* **2019**, *17* (2), 697−704.
(36) Fanta, F. T.; Dubale, A. A.; Bebizuh, D. F.; Atlabachew, M. Copper Doped Zeolite Composite for Antimicrobial Activity and Heavy Metal Removal from Waste Water. *BMC Chem.* **2019**, *13* (3), 1−12.
(37) Sen, T. K. Agricultural Solid Wastes Based Adsorbent Materials in the Remediation of Heavy Metal Ions from Water and Wastewater by Adsorption: A Review. *Molecules* **2023**, *28* (14), 5575.
(38) Sahu, S.; Pahi, S.; Tripathy, S.; Singh, S. K.; Behera, A.; Sahu, U. K.; Patel, R. K. Adsorption of Methylene Blue on Chemically Modified Lychee Seed Biochar: Dynamic, Equilibrium, and Thermodynamic Study. *J. Mol. Liq.* **2020**, *315*, No. 113743.
(39) Tseng, R. L.; Tran, H. N.; Juang, R. S. Revisiting Temperature Effect on the Kinetics of Liquid−Phase Adsorption by the Elovich Equation: A Simple Tool for Checking Data Reliability. *J. Taiwan Inst. Chem. Eng.* **2022**, *136* (May), No. 104403.
(40) Merrad, S.; Abbas, M.; Trari, M. Adsorption of Malachite Green onto Walnut Shells: Kinetics, Thermodynamic, and Regeneration of the Adsorbent by Chemical Process. *Fibers Polym.* **2023**, *24* (3), 1067−1081.
(41) Guo, H.; Zhang, S.; Kou, Z.; Zhai, S.; Ma, W.; Yang, Y. Removal of Cadmium(II) from Aqueous Solutions by Chemically Modified Maize Straw. *Carbohydr. Polym.* **2015**, *115*, 177−185.
(42) Dai, Y.; Sun, Q.; Wang, W.; Lu, L.; Liu, M.; Li, J.; Yang, S.; Sun, Y.; Zhang, K.; Xu, J.; Zheng, W.; Hu, Z.; Yang, Y.; Gao, Y.; Chen, Y.; Zhang, X.; Gao, F.; Zhang, Y. Utilizations of Agricultural Waste as Adsorbent for the Removal of Contaminants: A Review. *Chemosphere* **2018**, *211*, 235−253.
(43) Rehman, M. U.; Manan, A.; Uzair, M.; Khan, A. S.; Ullah, A.; Ahmad, A. S.; Wazir, A. H.; Qazi, I.; Khan, M. A. Physicochemical Characterization of Pakistani Clay for Adsorption of Methylene Blue: Kinetic, Isotherm and Thermodynamic Study. *Mater. Chem. Phys.* **2021**, *269*, No. 124722.
(44) Chen, X.; Hossain, M. F.; Duan, C.; Lu, J.; Tsang, Y. F.; Islam, M. S.; Zhou, Y. Isotherm Models for Adsorption of Heavy Metals from Water - A Review. *Chemosphere* **2022**, *307* (P1), No. 135545.
(45) Ayawei, N.; Ebelegi, A. N.; Wankasi, D. Modelling and Interpretation of Adsorption Isotherms. *J. Chem.* **2017**, *2017*, No. 3039817.
(46) Gubbuk, I. H. Isotherms and thermodynamics for the sorption of heavy metal ions onto functionalized sporopollenin. *Journal of Hazardous Materials.* **2011**, *186* (1), 416−422.
(47) Maneerung, T.; Liew, J.; Dai, Y.; Kawi, S.; Chong, C.; Wang, C. H. Activated Carbon Derived from Carbon Residue from Biomass Gasification and Its Application for Dye Adsorption: Kinetics, Isotherms and Thermodynamic Studies. *Bioresour. Technol.* **2016**, *200*, 350−359.
(48) Goswami, M.; Phukan, P. Enhanced Adsorption of Cationic Dyes Using Sulfonic Acid Modified Activated Carbon. *J. Environ. Chem. Eng.* **2017**, *5* (4), 3508−3517.
(49) Malima, N. M.; Owonubi, S. J.; Lugwisha, E. H.; Mwakaboko, A. S. Thermodynamic, isothermal and kinetic studies of heavy metals adsorption by chemically modified Tanzanian Malangali kaolin clay. *Int. J. Environ. Sci. Technol.* **2021**, *18*, 3153−3168.
(50) Shan, R. R.; Yan, L. G.; Yang, K.; Hao, Y. F.; Du, B. Adsorption of Cd(II) by Mg−Al−CO3- and magnetic Fe3O4/Mg−Al−CO3-layered double hydroxides: Kinetic, isothermal, thermodynamic and mechanistic studies. *J. Hazard. Mater.* **2015**, *299*, 42−49.
(51) Sarangi, N. V.; Rajkumar, R. Biosorption potential of Stoechospermum marginatum for removal of heavy metals from aqueous solution: Equilibrium, kinetic and thermodynamic study. *Chem. Eng. Res. Des.* **2024**, *203*, 207−218.

https://doi.org/10.1021/acsomega.4c06837
ACS Omega 2025, 10, 13816−13828